Journal of Power Sources 199 (2012) 287–292

Contents lists available at SciVerse ScienceDirect

Journal of Power Sources

journal homepage: www.elsevier.com/locate/jpowsour

The low and high temperature electrochemical performances of $Li_3V_2(PO_4)_3$/C cathode material for Li-ion batteries

Y.Q. Qiao, J.P. Tu*, X.L. Wang, C.D. Gu

State Key Laboratory of Silicon Materials and Department of Materials Science and Engineering, Zhejiang University, Hangzhou 310027, China

ARTICLE INFO

Article history:
Received 8 July 2011
Received in revised form 5 September 2011
Accepted 13 October 2011
Available online 20 October 2011

Keywords:
Lithium vanadium phosphate
Low temperature
High temperature
Lithium ion battery

ABSTRACT

$Li_3V_2(PO_4)_3$/C cathode material is synthesized by a carbon-thermal reduction method using polyvinyl alcohol as carbon source at 700 °C. The $Li_3V_2(PO_4)_3$/C electrode presents a high initial discharge capacity of 84.3, 111.1, 128.7, 129.2 and 132.1 mAh g^{-1} at −20, 0, 25, 40 and 65 °C between 3.0 and 4.3 V, and 118.9, 132.1, 187.6, 180.3 and 172.2 mAh g^{-1} between 3.0 and 4.8 V at 0.1 C, respectively. However, the electrode only delivers small discharge capacities at −20 °C at 10 C rate. The capacity fade at low temperatures is mainly attributed to the reduced ionic and electronic conductivity of the electrolyte, the increased impendence of solid electrolyte interface (SEI) and charge-transfer resistance on the electrolyte–electrode interfaces. At higher temperatures, the capacity increases with increasing temperature between 3.0 and 4.3 V, but decreases between 3.0 and 4.8 V. In the potential range of 3.0–4.8 V, the larger crystal structural distortion and non-uniformity of SEI layer at high temperatures may be the main reasons for the capacity loss.

© 2011 Elsevier B.V. All rights reserved.

1. Introduction

Lithium transition metal phosphates, $LiMPO_4$ (M = Fe, Co, Ni, Mn) [1–6] and $Li_3M'_2(PO_4)_3$ (M′ = Fe, V) [7,8] have been proposed as the most promising cathode materials for lithium-ion batteries. Among these materials, monoclinic $Li_3V_2(PO_4)_3$ has attracted considerable interest due to its high theoretical capacity, high operate voltage and good ion mobility [9–12]. Although it possesses so many advantages, $Li_3V_2(PO_4)_3$ as a cathode material still meets some drawbacks for practical implementation. One is the low electronic conductivity due to its intrinsic character [11]. Fortunately, carbon coating method can provide an effective way to solve the problem [13–21]. The carbons with various structures introduced by selecting carbon precursors have directly effect on the performance of the $Li_3V_2(PO_4)_3$/C composites. The selected carbon precursors are usually organics or polymers, such as citric acid [13,17], phenolic resin [14], humic acid [15], oxalic acid [20], stearic acid [21], polyethylene glycol (PEG) [16,22,23], sucrose [24], ascorbic acid [25] and glucose [26–28], etc. During the pyrolysis of organic/polymer precursors at high temperature in an inert atmosphere, some residual carbon may coat on the $Li_3V_2(PO_4)_3$ particles to form a conducting $Li_3V_2(PO_4)_3$/C composite. Wang et al. [16] employed polyethylene glycol (PEG) as a carbon precursor to prepare $Li_3V_2(PO_4)_3$/C cathode material which showed a high specific capacity, good rate capability and stable cycling ability. Jiang et al. [29] reported that the carbon coated $Li_3V_2(PO_4)_3$ exhibited a good cycling performance when employed PVA-2000 as the carbon source by sol-gel method at 750 °C. Recently, Wang et al. [30] synthesized $Li_3V_2(PO_4)_3$/C composite using PVA as carbon source at 850 °C, and the material exhibited an excellent long-term cyclability.

In practical applications, it is proposed that the Li-ion batteries are required to operate at various temperatures. At low temperatures (below 0 °C), the problems have been summarized by Zhang et al. [31] such as the increased charge-transfer resistance on the electrolyte–electrode interfaces, high polarization, limited diffusivity of lithium ions, reduced ionic conductivity of the electrolyte and solid electrolyte interface (SEI) formed on the electrodes. At high temperatures, however, the Li-ion batteries may also suffer from capacity fading due to the non-uniformity of SEI layer, electrolyte decomposition, current collector corrosion and/or nanocrystalline deposits and phase segregation in the cathode [32]. Until recently, there have been only a few works on the electrochemical performance at low and high temperatures for $Li_3V_2(PO_4)_3$ cathode material. Chen et al. [18] found that the $Li_3V_2(PO_4)_3$ electrode could present a large reversible capacity and good cyclic stability at 55 °C between 3.0 and 4.3 V. Recently, Rui et al. [33] reported that the $Li_3V_2(PO_4)_3$/C electrode could deliver a high stable reversible discharge capacity of 108.1 mAh g^{-1} at −20 °C in the potential range of 3.0–4.3 V at 0.3 C rate.

In the present work, we propose to use PVA-124 as a carbon source to produce $Li_3V_2(PO_4)_3$/C composite by a simple carbon-thermal reduction method. It is anticipated that the carbon from pyrolysis of PVA can be *in situ* formed on the surface of $Li_3V_2(PO_4)_3$

* Corresponding author. Tel.: +86 571 87952856; fax: +86 571 87952573.
E-mail address: tujp@zju.edu.cn (J.P. Tu).

0378-7753/$ – see front matter © 2011 Elsevier B.V. All rights reserved.
doi:10.1016/j.jpowsour.2011.10.054

particles which results in a fine carbon coating and uniform particle size distribution at a proper sintering temperature. Herein, the electrochemical properties of the carbon coated $Li_3V_2(PO_4)_3$ at various temperatures (−20, 0, 25, 40 and 65 °C) in the potential ranges of 3.0–4.3 V and 3.0–4.8 V were systematically investigated.

2. Experimental

$Li_3V_2(PO_4)_3$/C powder was synthesized by a carbon-thermal reduction method using NH_4VO_3, $NH_4H_2PO_4$ and Li_2CO_3 as the starting materials. An appropriate amount of PVA-124 as a carbon source was added to the raw materials. A mixture of the raw materials and PVA-124 was planetary milled in alcohol for 8 h. The obtained mixture was dried in an oven to evaporate alcohol. Then, it was placed in a porcelain boat and sintered at 700 °C for 8 h under Ar flow in a tube furnace to get $Li_3V_2(PO_4)_3$/C composite.

DSC–TGA analysis of the precursor after ball-milling was performed between room temperature and 1000 °C at a heating rate of 10 °C min^{-1} under an Ar flow of 120 ml min^{-1}. The microstructure and morphology of the product were characterized by X-ray diffraction (XRD, Philips PC-APD with Cu K radiation), X-ray photoelectron spectroscopy (XPS, AXIS UTLTRADLD equipped with a dual Mg Kα–Al Kα anode for photoexcitation), field emission scanning electron microscopy (FESEM, FEI SIRION) and transmission electron microscopy (TEM, Tecnai G2 F30 S-Twin). The residual carbon content of the powder was determined by means of an automatic elemental analyzer (EA, Flash EA1112). Raman scattering spectroscopy (LABRAM HR-800) was recorded at room temperature with the wave number shift from 4000 to 100 cm^{-1} in ultraviolet laser excitation line of 325 nm.

For electrochemical tests, the cathodes consisted of active material (85%), carbon conductivity (10%) and PVDF binder (5%) on Al foil current collector. Lithium foil was used as the anode. 1 M $LiPF_6$ in ethylene carbonate (EC)-diethyl carbonate (DEC) (1:1 in volume) as the electrolyte, and a polypropylene micro-porous film (Cellgard 2300) as the separator. The cells were assembled under pure argon atmosphere in a glove box. The charge–discharge tests were carried out on LAND battery program-control test system in the potential ranges of 3.0–4.3 V and 3.0–4.8 V at charge–discharge rates from 0.1 to 10 C at various temperatures (−20, 0, 25, 40 and 65 °C), respectively. Cyclic voltammetry (CV) experiments were performed on a CHI660C electrochemical workstation in the potential ranges of 3.0–4.3 V and 3.0–4.8 V (vs. Li/Li^+) at various temperatures at a scan rate of 0.1 mV s^{-1}, respectively. A three-electrode cell was used for EIS tests, where lithium foils acted as both the counter and reference electrodes. EIS measurements were also recorded on this electrochemical workstation with the frequency ranging from 10 kHz to 10 mHz by applying an AC voltage of 5 mV at −20, 0, 25, 40 and 65 °C.

3. Results and discussion

Fig. 1 shows DSC–TGA curves of the precursor after ball-milling from room temperature to 1000 °C. The TGA curve shows several main weight loss steps over the temperature range. The first step occurred from room temperature to 115 °C is attributed to the release of absorbed water. It has been previously reported that the pyrolysis of PVA in a nitrogen gas flow starts at 160 °C and begins to abruptly decompose at 280 °C [34]. Therefore, the second step between 115 and 250 °C is mainly related to the evaporation of water and ammonia from the precursor. The following step between 250 and 600 °C can be ascribed to the pyrolysis of PVA. From 600 to 800 °C, there is no obvious weight loss in TGA curve. During this process, the well-crystallized $Li_3V_2(PO_4)_3$/C composite can be obtained from the reaction of lithium oxide, vanadium oxide, phosphate and excess carbon. Above 800 °C, the weight loss turns evident again, which may be attributed to some side reactions lead to $Li_3V_2(PO_4)_3$ decomposition. By following the results of DSC–TGA, the precursor was sintered at 700 °C for 10 h under Ar flow.

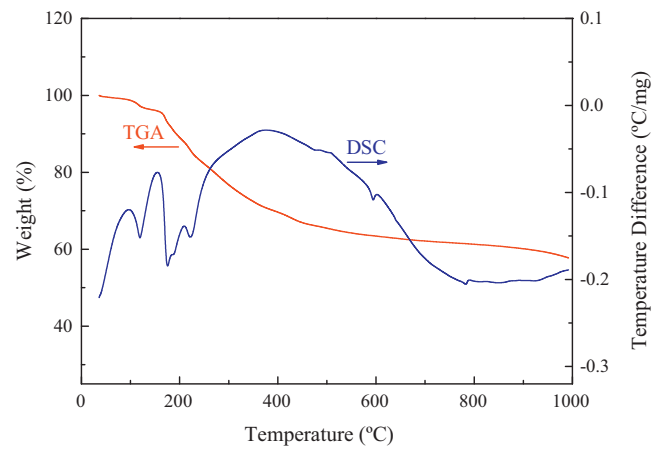

Fig. 1. DSC–TGA curves of the $Li_3V_2(PO_4)_3$/C precursor recorded from room temperature to 1000 °C at a heating rate of 10 °C min^{-1} under an Ar flow of 120 ml min^{-1}.

Fig. 2 shows XRD pattern of the $Li_3V_2(PO_4)_3$/C composite synthesized at 700 °C. It is found that all the diffraction peaks can be indexed as pure and well-crystallized $Li_3V_2(PO_4)_3$ phase with a monoclinic structure (ICSD #96962). According to the results of structure refinement, the $Li_3V_2(PO_4)_3$ phase has lattice parameters with a = 0.8606 nm, b = 0.8598 nm, c = 1.2040 nm and β = 90.58°, which are consistent well with the values reported previously [10,14]. As shown in Fig. 2, there is no additional diffraction peak related-carbon in the XRD pattern, which indicates that the carbon generated from PVA is amorphous or too thin on the $Li_3V_2(PO_4)_3$ particles. However, the amount of residual carbon is detected by elemental analysis in the composite is 4.63 wt.%. The XPS spectrum of the $Li_3V_2(PO_4)_3$/C composite is illustrated in Fig. 3. According to the published reports [18,35,36], the binding energy of 133.08, 284.62, 517.32 and 530.58 eV corresponds to P 2p, C ls, V 2p3 and O 1s, respectively. Hence, it can be concluded that the product only consisted of V^{3+}, P^{5+}, O^{2-} and carbon.

Fig. 4a shows the SEM image of the $Li_3V_2(PO_4)_3$/C composite. The powder has uniform particle size distribution with little agglomeration. In order to check the carbon coating on the particles, the powder was analyzed by TEM. Fig. 4b and c show the TEM

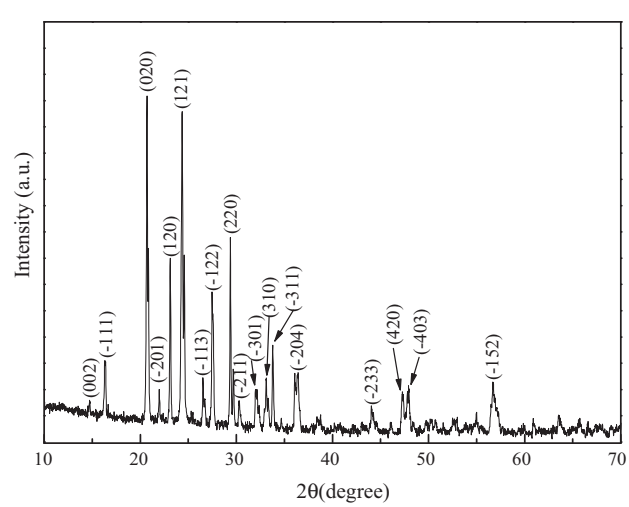

Fig. 2. XRD pattern of $Li_3V_2(PO_4)_3$/C synthesized at 700 °C.

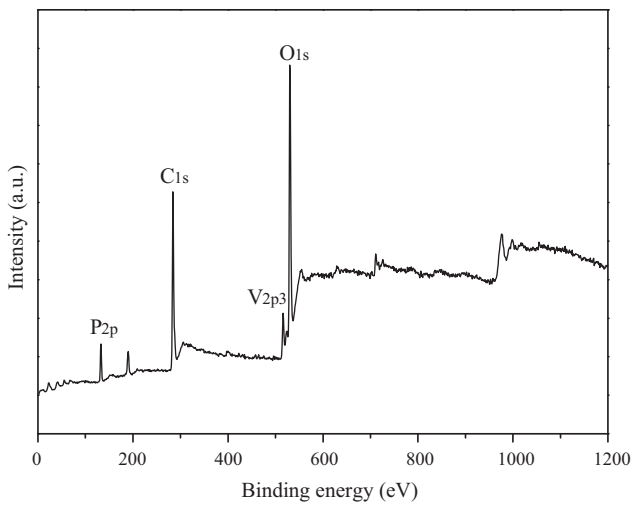

Fig. 3. XPS spectrum of $Li_3V_2(PO_4)_3$/C.

and HRTEM images of the $Li_3V_2(PO_4)_3$/C composite. From these images, a uniform carbon coating with a thickness of about 10 nm can be observed on the particle surface. In the body part of the particle, the lattice fringes are clearly visible. The spacing of the fringes is measured to be 0.367 nm, which corresponds well with the d-spacing of (1 1 2) crystal face. The carbon coating appears to be amorphous. And the presence of this carbon layer is believed to impede the grain growth of $Li_3V_2(PO_4)_3$ as well as provide good electrical contact between the particles. Based on the above structure and morphology analysis, the carbon from pyrolysis of PVA can be *in situ* formed on the surface of fresh $Li_3V_2(PO_4)_3$ particles to form a carbon web structure and lead to a uniform size distribution. Fig. 4d shows the Raman spectrum of the $Li_3V_2(PO_4)_3$/C composite in the range of 900–1800 cm^{-1}. In the spectrum, two intense broad bands at 1596.8 cm^{-1} and 1356.2 cm^{-1} are attributed to the graphite band (G-band) and the disorder-induced phonon mode (D-band), respectively. The I_D/I_G value of the $Li_3V_2(PO_4)_3$/C composite is about 0.87, suggesting that the graphite-like carbon in the residual carbon is about 50%, which is helpful for improving the electronic conductivity and electrochemical performance of $Li_3V_2(PO_4)_3$ [16,37]. Therefore, it is expected that the efficient carbon-coated $Li_3V_2(PO_4)_3$ composite would exhibit favorable electrochemical properties. In addition, there are three broad Raman bands at 1138.7, 1045.9 and 1005.8 cm^{-1}, which can be indexed to the vibrations of $Li_3V_2(PO_4)_3$ [38].

Fig. 5 shows the first charge–discharge curves and rate performance of $Li_3V_2(PO_4)_3$/C at different temperatures in the potential ranges of 3.0–4.3 V and 3.0–4.8 V. At higher temperatures (above 25 °C), the electrode exhibits three charge flat plateaus around 3.60, 3.67 and 4.07 V and three discharge flat plateaus around 3.58, 3.66 and 4.05 V (Fig. 5a), which are identified as the two-phase transition processes during the electrochemical reactions [8,10]. As the operation temperature decreases to 0 °C and −20 °C, the potential differences between the charge and discharge plateaus increase and the capacities reduce, indicating an increased electrical polarization. Between 3.0 and 4.3 V, the $Li_3V_2(PO_4)_3$/C electrode presents an initial discharge capacity of 84.3, 111.1, 128.7, 129.2 and 132.1 mAh g^{-1} at −20, 0, 25, 40 and 65 °C at 0.1 C rate, respectively (Fig. 5a and b). At 10 C rate, the electrode can still deliver a discharge capacity of 93.8, 117.2, 119.7 and 129.4 mAh g^{-1} at 0, 25, 40 and 65 °C, respectively. However, the electrode only delivers a discharge capacity of 3.6 mAh g^{-1} at −20 °C at 10 C rate. As the current density decreases to 0.1 C, the $Li_3V_2(PO_4)_3$/C electrode shows high discharge capacity recovery such as 95.6 mAh g^{-1} at −20 °C. It is found that the discharge capacities increase with increasing the operation temperature between 3.0 and 4.3 V at various current densities. In the potential range of 3.0–4.8 V, as the

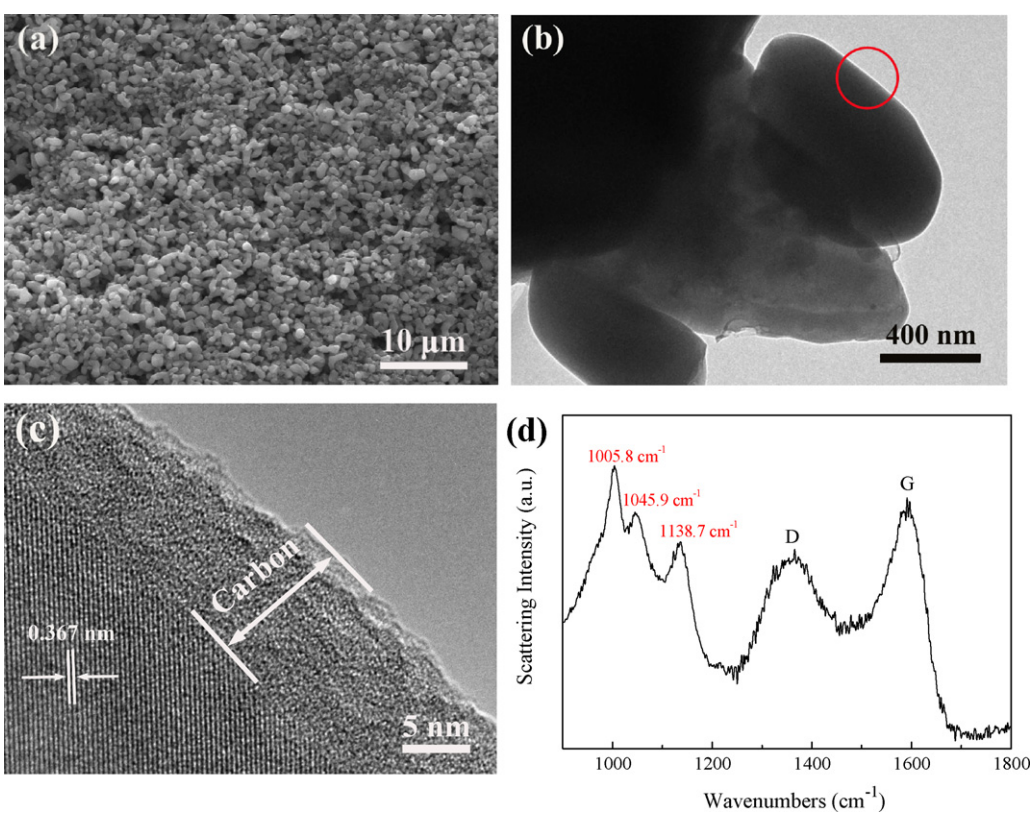

Fig. 4. (a) SEM, (b) TEM, (c) HRTEM images, and (d) Raman scattering spectrum of $Li_3V_2(PO_4)_3$/C synthesized at 700 °C.

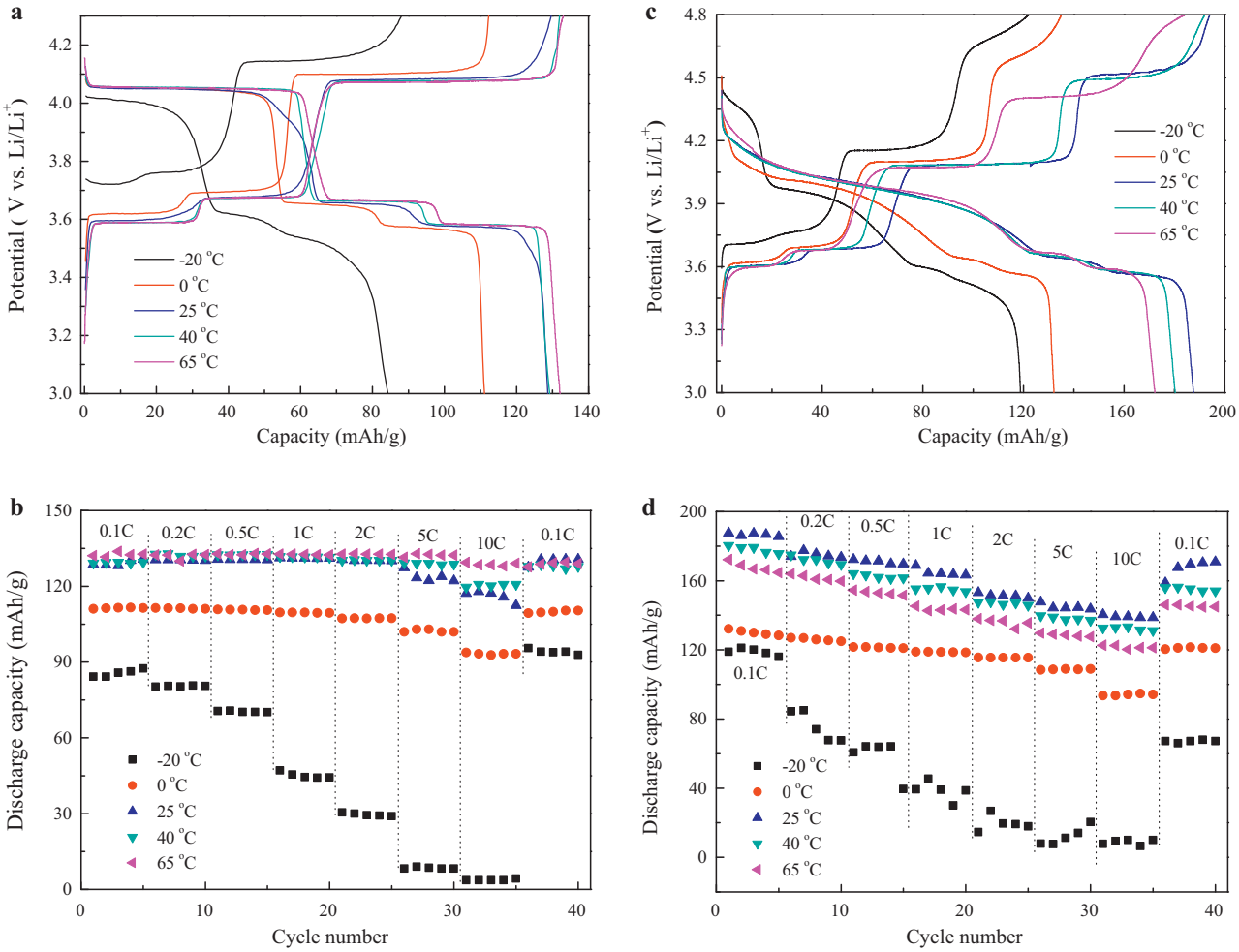

Fig. 5. (a) The first charge–discharge curves at 0.1 C and (b) rate performance of $Li_3V_2(PO_4)_3$/C at different temperatures between 3.0 and 4.3 V; (c) the first charge–discharge curves at 0.1 C; and (d) rate performance of $Li_3V_2(PO_4)_3$/C at different temperatures between 3.0 and 4.8 V.

operation temperature increases, the potential differences between the charge and discharge plateaus decrease (Fig. 5c), similar to the behavior between 3.0 and 4.3 V. The $Li_3V_2(PO_4)_3$/C electrode presents an initial discharge capacity of 118.9, 132.1, 187.6, 180.3 and 172.2 mAh g^{-1} at −20, 0, 25, 40 and 65 °C at 0.1 C rate, respectively (Fig. 5c and d). Unfortunately, at −20 °C, the discharge capacity of the electrode decreases sharply with the increase of charge–discharge rate between 3.0 and 4.8 V. The cell only delivers a discharge capacity of 7.8 mAh g^{-1} at −20 °C at 10 C rate. At 40 and 65 °C, the discharge capacities are lower than that at 25 °C. Cycling the cell to a higher voltage, i.e., 4.8 V, means extraction of all the 3 Li^+ from $Li_3V_2(PO_4)_3$. This leads the crystal structure of $V_2(PO_4)_3$ and $LiV_2(PO_4)_3$ is twisted during the phase transition process at the high voltage. Therefore, at higher operation temperatures, the larger crystal structural distortion and non-uniformity of SEI layer may cause the re-insertion of Li^+ into the host structure relatively difficult during the discharge process. Thus, the electrode displays lower capacities at higher temperatures between 3.0 and 4.8 V.

CV curves of the $Li_3V_2(PO_4)_3$/C electrode in the potential ranges of 3.0–4.3 V and 3.0–4.8 V at different temperatures are shown in Fig. 6. It is clearly seen that the electrode present three couples of oxidation and reduction peaks between 3.0 and 4.3 V (Fig. 6a, labeled as a′/a, b′/b and c′/c), while in the potential range of 3.0–4.8 V, four oxidation peaks (labeled as d′, e′, f′ and g) and three reduction peaks (Fig. 6b, labeled as d–f). Between 3.0 and 4.3 V, with increasing the operation temperature, the peak of current density of the electrode increases significantly. Meanwhile, the potential differences between oxidation and reduction peaks tend to smaller with increasing the temperature, as summarized in Table 1. However, between 3.0 and 4.8 V, the potential differences between oxidation and reduction peaks also become smaller with increasing the temperature (Fig. 6b and Table 1), but the peaks of current density of the electrode at 40 and 65 °C are lower than that at 25 °C, indicating lower capacity delivered. These results are in good agreement with the charge–discharge plateaus presented in Fig. 5a and b. Thus, we may conclude that the higher operation temperature can decrease the potential differences of the electrode, but cannot improve the capacity in the potential range of 3.0–4.8 V.

In order to understand the impedance changes of the $Li_3V_2(PO_4)_3$/C composite at different operation temperatures, EIS measurements were conducted at various temperatures after 5 cycles. Fig. 7a presents the Nyquist plots of the $Li_3V_2(PO_4)_3$/C electrode at a stage of discharge (3.6 V) at different operation temperatures. It can be found that the Nyquist plots consist of a small intercept at high frequency, two partially overlapped semicircles at high and medium frequency, and a linear part in the low frequency. Fig. 7b presents an equivalent circuit to simulate the electrochemical impedance data. R_{el} represents the solution resistance; R_{sl} and C_{sl} designate the Li^+ migration resistance and capacity of surface layer, respectively; R_{ct} and C_{dl} stand for the related charge-transfer resistance and double-layer capacitance, respectively; Z_W represents the diffusion-controlled Warburg impedance [39–41]. The evaluated impedance parameters according to the equivalent circuit of Fig. 7b and the apparent diffusion coefficients of Li ions at

Table 1
Potential differences between the oxidation and reduction peaks for $Li_3V_2(PO_4)_3$/C electrode (Fig. 6).

T (°C)	$\Delta E_{a'-a}$ (V)	$\Delta E_{b'-b}$ (V)	$\Delta E_{c'-c}$ (V)	$\Delta E_{d'-d}$ (V)	$\Delta E_{e'-e}$ (V)	$\Delta E_{f'-f}$ (V)	ΔE_{g-f} (V)
−20	0.251	0.230	0.317	0.158	0.162	0.323	0.816
0	0.162	0.151	0.195	0.108	0.101	0.221	0.715
25	0.096	0.092	0.134	0.102	0.077	0.065	0.633
40	0.075	0.081	0.113	0.075	0.071	0.064	0.612
65	0.091	0.082	0.110	0.041	0.042	0.052	0.550

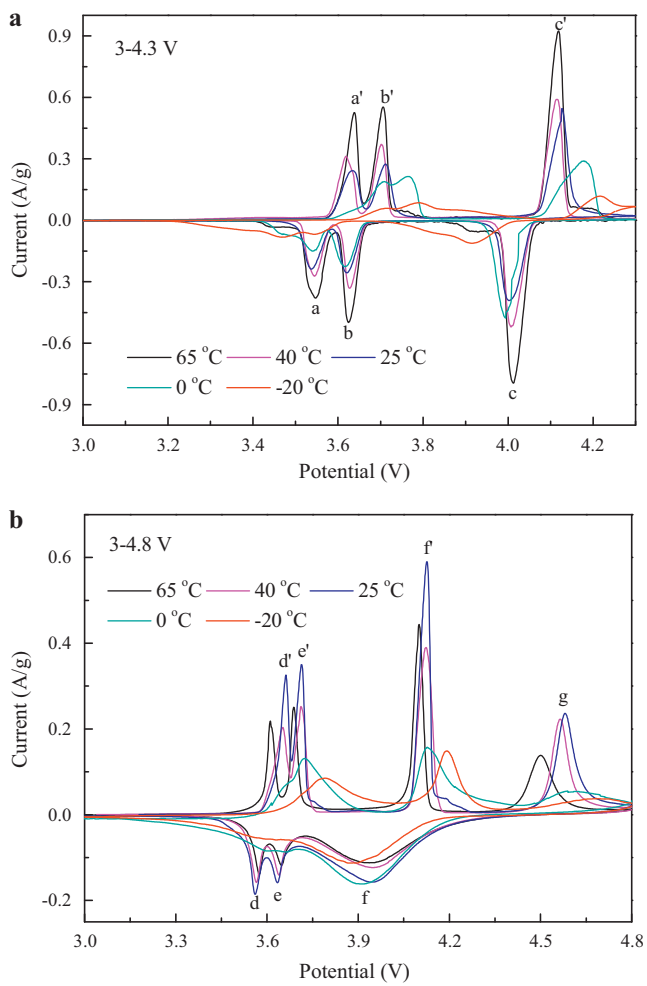

Fig. 6. CV curves of $Li_3V_2(PO_4)_3$/C electrode in the potential ranges of (a) 3.0–4.3 V and (b) 3.0–4.8 V at different temperatures. Scan rate: 0.1 mV s^{-1}.

different temperatures are presented in Table 2 and Fig. 8. It can be seen that R_{el} and R_{sl} of the $Li_3V_2(PO_4)_3$/C electrode increase with decreasing the temperature, indicating the reduced ionic and electronic conductivity of the electrolyte and the increased impendence of solid electrolyte interface (SEI). Notably, the values of R_{ct} increase more rapidly with decreasing the temperature than those of R_{el} and R_{sl} (Table 2 and Fig. 8). It is seen that the charge-transfer resistance on the electrolyte–electrode interfaces is one of the uppermost reasons for the poor low-temperature performance of the electrode [31].

The inclined line in the low frequency represents the diffusion of lithium ions into the bulk of electrode material or so-called Warburg diffusion. The obtained apparent diffusion coefficients of Li^+ at different temperatures are listed in Table 2. As shown in Fig. 9, the relationship between diffusion coefficient of Li^+ (D_{Li^+}) and temperature shows a format as: $\text{Log}\, D_{Li^+} = -1.8655 - (2334.01/T)$, which follows the conventional Arrhenius equation [33]. The apparent activation energies (E_a) for lithium intercalation can be estimated by EIS [33,42]. The apparent activation energy ($E_a = -Rk \ln 10$, R is the gas constant and k is the slope of the fitting line shown in Fig. 9) of the $Li_3V_2(PO_4)_3$/C composite is calculated to be 44.7 kJ mol^{-1}. Although the activation energy $Li_3V_2(PO_4)_3$/C composite is lower than that of $LiFePO_4$/C [33] that indicates the enhanced kinetics of lithium-ion diffusion, the low and high temperature performances

Table 2
Evaluated impedance parameters according to the equivalent circuit of Fig. 7b and the apparent diffusion coefficients of Li ions at different temperatures.

T (°C)	R_{el} (Ω)	R_{sl} (Ω)	R_{ct} (Ω)	D_{Li^+} ($cm^2\ s^{-1}$)
−20	16.33	21.46	335.5	1.01×10^{-11}
0	13.93	15.30	139.6	3.18×10^{-11}
25	11.65	9.29	37.20	3.02×10^{-10}
40	12.85	7.84	10.19	1.68×10^{-10}
65	9.42	2.24	3.26	3.10×10^{-9}

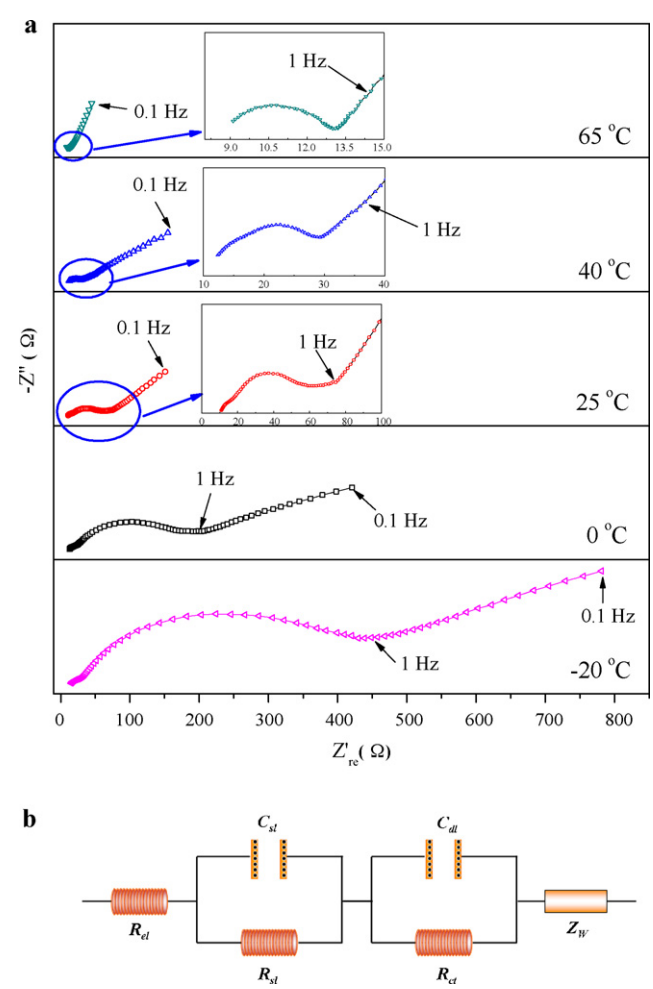

Fig. 7. (a) Nyquist plots for the $Li_3V_2(PO_4)_3$/C composite at a stage of discharge (3.6 V) at different operation temperatures and (b) equivalent circuit used for simulating the experimental impedance data.

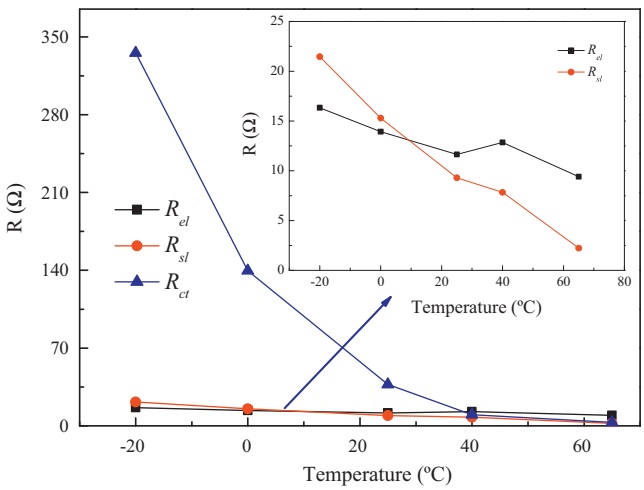

Fig. 8. Temperature dependence of R_{el}, R_{sl} and R_{ct} of $Li_3V_2(PO_4)_3$/C electrode.

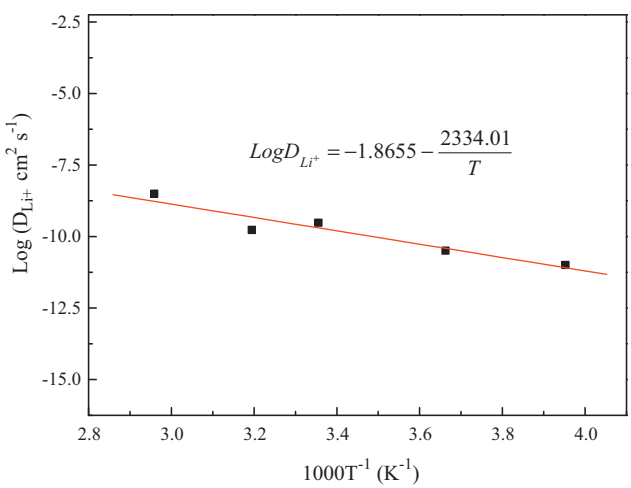

Fig. 9. Arrhenius plot of the apparent diffusion coefficients of lithium ions in $Li_3V_2(PO_4)_3$/C composite.

of the material still need to be further improved especially at higher current densities such as at 5 C and 10 C.

4. Conclusions

The well carbon coated $Li_3V_2(PO_4)_3$ cathode material has been successfully synthesized by a carbon-thermal reduction method using PVA-124 as a carbon source. At −20 °C, the $Li_3V_2(PO_4)_3$/C electrode can deliver an high initial discharge capacity of 84.3 and 118.9 mAh g^{-1} at 0.1 C in the potential ranges of 3.0–4.3 V and 3.0–4.8 V, respectively. EIS analysis reveals that with the decrease of temperature, the charge-transfer resistance (R_{ct}) becomes significantly higher than the solution resistance (R_{el}) and the Li^+ migration resistance (R_{sl}). Therefore, R_{ct} is considered to be a predominant factor to influence the capacity of the electrode at low temperatures. At higher temperatures (25, 40 and 65 °C), the capacity increases with increasing the temperature between 3.0 and 4.3 V, but decreases between 3.0 and 4.8 V. This would be mainly resulted from the larger crystal structural distortion and non-uniformity of SEI layer at high temperatures.

References

[1] A.K. Padhi, K.S. Najundaswamy, J.B. Goodenough, J. Electrochem. Soc. 144 (1997) 1188.
[2] K. Amine, H. Yasuda, M. Yamachi, Electrochem, Solid State Lett. 3 (2000) 178.
[3] J. Wolfenstine, J. Allen, J. Power Sources 136 (2004) 150.
[4] S.K. Martha, B. Markovsky, J. Grinblat, Y. Gofer, O. Haik, E. Zinigrad, D. Aurbach, T. Drezen, D. Wang, G. Deghenghi, I. Exnarb, J. Electrochem. Soc. 156 (1997) A514.
[5] J.Y. Xiang, J.P. Tu, L. Zhang, X.L. Wang, Y. Zhou, Y.Q. Qiao, Y. Lu, J. Power Sources 195 (2010) 8331.
[6] W.L. Liu, J.P. Tu, Y.Q. Qiao, X.L. Wang, J.P. Zhou, S.J. Shi, C.D. Gu, J. Power Sources 195 (2011) 7728.
[7] S. Zhu, H. Zhou, T. Miyoshi, M. Hibino, I. Honma, M. Ichihara, Adv. Mater. 16 (2004) 2012.
[8] S.-C. Yin, H. Grondey, P. Strobel, H. Huang, L.F. Nazar, J. Am. Chem. Soc. 125 (2003) 326.
[9] L. Zhang, X.L. Wang, J.Y. Xiang, Y. Zhou, S.J. Shi, J.P. Tu, J. Power Sources 195 (2010) 5057.
[10] M.Y. Saïdi, J. Barker, H. Huang, J.L. Swoyer, G. Adamson, J. Power Sources 119–121 (2003) 266.
[11] M.M. Ren, Z. Zhou, X.P. Gao, W.X. Peng, J.P. Wei, J. Phys. Chem. C 112 (2008) 5689.
[12] Y.Q. Qiao, J.P. Tu, Y.J. Mai, J.Y. Xiang, X.L. Wang, C.D. Gu, J. Alloys Compd. 509 (2011) 7181.
[13] X.H. Rui, C. Li, C.H. Chen, Electrochim. Acta 54 (2009) 3374.
[14] P. Fu, Y.M. Zhao, Y.Z. Dong, X.N. An, G.P. Shen, J. Power Sources 162 (2006) 651.
[15] X.C. Zhou, Y.M. Liu, Y.L. Guo, Electrochim. Acta 54 (2009) 2253.
[16] J.W. Wang, J. Liu, G.L. Yang, X.F. Zhang, X.D. Yan, X.M. Pan, R.S. Wang, Electrochim. Acta 54 (2009) 6451.
[17] Y.Z. Li, Z. Zhou, X.P. Gao, J. Yan, Electrochim. Acta 52 (2007) 4922.
[18] Q.Q. Chen, J.M. Wang, Z. Tang, W.C. He, H.B. Shao, J.Q. Zhang, Electrochim. Acta 52 (2007) 5251.
[19] X.J. Zhu, Y.X. Liu, L.M. Geng, L.B. Chen, J. Power Sources 184 (2008) 578.
[20] J.-C. Zheng, X.-H. Li, Z.-X. Wang, H.-J. Guo, Q.-Y. Hu, W.-J. Peng, J. Power Sources 189 (2009) 476.
[21] Y.Q. Qiao, X.L. Wang, J.Y. Xiang, D. Zhang, W.L. Liu, J.P. Tu, Electrochim. Acta 56 (2011) 2269.
[22] C.X. Chang, J.F. Xiang, X.X. Shi, X.Y. Han, L.J. Yuan, J.T. Sun, Electrochim. Acta 53 (2008) 2232.
[23] X.Y. Wang, S.Y. Yin, K.L. Zhang, Y.X. Zhang, J. Alloys Compd. 486 (2009) L5.
[24] T. Jiang, C. Wang, G. Chen, H. Chen, Y. Wei, X. Li, Solid State Ionics 180 (2009) 708.
[25] Y.Q. Qiao, J.P. Tu, J.Y. Xiang, X.L. Wang, Y.J. Mai, D. Zhang, W.L. Liu, Electrochim. Acta 56 (2011) 4139.
[26] Y.N. Ko, H.Y. Koo, J.H. Kim, J.H. Yi, Y.C. Kang, J.-H. Lee, J. Power Sources 196 (2011) 6682.
[27] C.X. Chang, J.F. Xiang, X.X. Shi, X.Y. Han, L.J. Yuan, J.T. Sun, Electrochim. Acta 54 (2008) 623.
[28] P. Fu, Y.M. Zhao, X.N. An, Y.Z. Dong, X.M. Hou, Electrochim. Acta 52 (2007) 5281.
[29] T. Jiang, W.C. Pan, J. Wang, X.F. Bie, F. Du, Y.J. Wei, C.Z. Wang, G. Chen, Electrochim. Acta 55 (2010) 3864.
[30] J.W. Wang, X.F. Zhang, J. Liu, G.L. Yang, Y.C. Ge, Z.J. Yu, R.S. Wang, X.M. Pan, Electrochim. Acta 55 (2010) 6879.
[31] S.S. Zhang, K. Xu, T.R. Jow, J. Power Sources 115 (2003) 137.
[32] J. Shim, R. Kostecki, T. Richardson, X. Song, K.A. Striebel, J. Power Sources 112 (2002) 222.
[33] X.H. Rui, Y. Jin, X.Y. Feng, L.C. Zhang, C.H. Chen, J. Power Sources 196 (2011) 2109.
[34] C. Nakajima, T. Saito, T. Yamaya, M. Shimoda, Fuel 77 (1998) 321.
[35] H.W. Liu, C.X. Cheng, X.T. Huang, J.L. Li, Electrochim. Acta 55 (2010) 8461.
[36] M.M. Ren, Z. Zhou, Y.Z. Li, X.P. Gao, J. Yan, J. Power Sources 162 (2006) 1357.
[37] Y.Q. Qiao, J.P. Tu, X.L. Wang, D. Zhang, J.Y. Xiang, Y.J. Mai, C.D. Gu, J. Power Sources 196 (2011) 7715.
[38] C.M. Burba, R. Frech, Solid State Ionics 177 (2007) 3445.
[39] J.S. Huang, L. Yang, K.Y. Liu, Y.F. Tang, J. Power Sources 195 (2010) 5013.
[40] D. Aurbach, B. Markovsky, M.D. Levi, E. Levi, A. Schechter, M. Moshkovich, Y. Cohen, J. Power Sources 81–82 (1999) 95.
[41] Y.Q. Qiao, X.L. Wang, Y. Zhou, J.Y. Xiang, D. Zhang, S.J. Shi, J.P. Tu, Electrochim. Acta 56 (2010) 510.
[42] H. Ma, Z.Q. Yuan, F.Y. Cheng, J. Liang, Z.L. Tao, J. Chen, J. Alloys Compd. 509 (2011) 6030.